Nano-Manipulation Based on Real-Time Compressive Tracking

Gongxin Li, Wenxue Wang, *Member, IEEE*, Yuechao Wang, *Member, IEEE*, Shuai Yuan, Wenguang Yang, Ning Xi, *Fellow, IEEE*, and Lianqing Liu, *Member, IEEE*

***Abstract*—Quick tracking in nano-manipulation has been attracting increasing attention among scientific researchers and engineers because it can significantly enhance the effectiveness and efficiency of nano-manipulation. The main reasons that hinder the improvement of accuracy and efficiency of nano-manipulation are the lack of effective real-time tracking and unavoidable perturbations by uncertainties and nonlinearities in the manipulation system. In this paper, we present a new strategy based on compressive sensing to realize quick real-time tracking nano-manipulation trajectory, and build a new kinematic model for objects to be manipulated to overcome the effect of tip positioning and contacting biases on nano-manipulation with AFM. With this approach, the deviation of the object from the predesigned trajectory during the manipulation can be corrected with up to two-thirds of time less than the traditional method, and the object can be smoothly moved to any destination in the nano-space. The approach requires no priori knowledge about the system, environment, and objects being manipulated. It is validated that this strategy works for both hard regular objects and soft irregular samples by experiments.**

***Index Terms*—Nano-manipulation, compressive sensing, compressive tracking, local imaging.**

I. Introduction

ATOMIC force microscopy (AFM) [1] is an emerging technology that has drawn considerable attention as a practical tool for observing sample surface topography at micro/nano-scale. Recently, AFM has been widely utilized for nano-manipulation through Van der Waals force or mechanical force between AFM probe tip and samples. Many AFM-based approaches for nano-manipulation have been proposed to successfully manipulate targets at nano-scale [2]–[4], and overall, these approaches consist of four steps: acquiring image of interest region, designing offline strategy for nano-manipulation, manipulating nano-targets with AFM, and validating the nano-manipulation results.

One of main issues for AFM-based nano-manipulation is to improve its accuracy and efficiency. The critical reason that hinders the improvement of nano-manipulation accuracy and efficiency is that the nano-manipulation is essentially a blind process and lacks effective real-time tracking. It is hard to realize real-time visual observation of the object and its status due to the complexity of the AFM system and confinement of the nano-space of manipulation. There is an integrated optical microscopy within the AFM system, but it is mainly used to position AFM tip and locate samples. Although some studies have reported that AFM-based robotic systems have been used to manipulate particles or fabricate nano-structures successfully under the optical microscopy [3], [5], the optical microscopy cannot be used for observing the interaction between the tip and samples since the tip is under the AFM cantilever, and hence it cannot be used for tracking the nano-manipulation process. Furthermore, if the size of the object to be manipulated is smaller than that of the optical diffraction extremity, then it would be difficult to recognize the object shape and location through the optical microscopy due to the dynamic changes of nano-environment caused by uncertainties such as thermal drift.

Another solution to track nano-manipulation is the utilization of haptic device as a force sensor. In some studies, the haptic device has been assembled into the AFM system to realize the precise manipulation by feeling the interaction between the AFM tip and the object [6]. Although the force feedback is real-time, this approach can sense the interaction only, and neither force orientation nor dynamic status of objects being manipulated can be detected. Therefore the force feedback with a haptic device is not an effective tracking strategy for nano-manipulation. To overcome the limitation of the force feedback with haptic device as above, an AFM-based interactive nano-manipulation system with force and visual feedbacks has been developed to sense real-time 3-D nano-forces from the AFM tip and to observe the dynamic changes of nano-environments during the manipulations of multi-wall carbon nanotube [7], [8]. In this strategy, AFM cantilever is used as a nano-force sensor and the 3-D nano-force is derived from the cantilever's bending and twisting deflections. However, the accuracy of 3-D nano-force is heavily dependent on the parameters of AFM system and cantilever, such as elastic coefficient of cantilever, which are hard to obtained or calibrated. With respective to the visual feedback, the visual information provided to the operator, such as tip position and applied force, is acquired by modeling manipulation process based on virtual reality technology. So the visual information significantly relies on modeling accuracy and nano-force

Manuscript received December 11, 2014; revised April 15, 2015; accepted June 20, 2015. Date of publication June 25, 2015; date of current version September 3, 2015. The review of this paper was arranged by Associate Editor F. Lombardi. This work was supported by the National Natural Science Foundation of China under Grant 61327014 and Grant 61305125, the National High Technology Research and Development Program of China under Grant 2012AA020103, and the CAS/SAFEA International Partnership Program for Creative Research Teams.

G. Li and W. Yang are with the State Key Laboratory of Robotics, Shenyang Institute of Automation, Chinese Academy of Sciences, Shenyang 110016, China, and also with the University of the Chinese Academy of Sciences, Beijing 100049, China (e-mail: ligongxin@sia.cn; yangwenguang@sia.cn).

W. Wang, Y. Wang, and L. Liu are with the State Key Laboratory of Robotics, Shenyang Institute of Automation, Chinese Academy of Sciences, Shenyang 110016, China (e-mail: wangwenxue@sia.cn; ycwang@sia.cn; lqliu@sia.cn).

S. Yuan is with the Information and Control Engineering Faculty, Shenyang Jianzhu University, Shenyang 110016, China (e-mail: reidyuan@163.com).

N. Xi is with the Department of Mechanical and Biomedical Engineering, City University of Hong Kong, Hong Kong (e-mail: ningxi@sia.cn).

Color versions of one or more of the figures in this paper are available online at http://ieeexplore.ieee.org.

Digital Object Identifier 10.1109/TNANO.2015.2449871

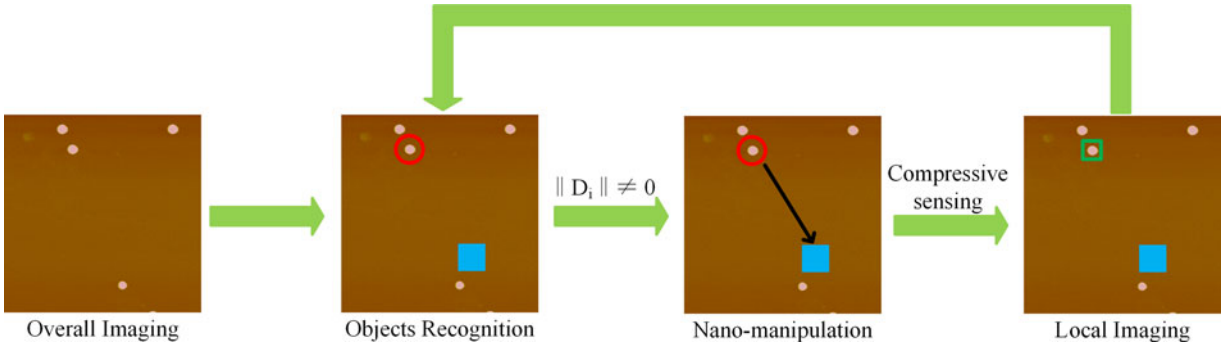

Fig. 1. The process of nano-manipulation with compressive tracking consists four procedures: Overall imaging, object recognition nano-manipulation and local imaging. The local image acquired in the procedure of local imaging strategy is fed back to the procedure of object recognition to identify the new location of the object and compute the new distance and deviation for next manipulation. The blue solid square denotes the destination location, the red circle denotes the object to be manipulated and the green hollow block denotes the range of local imaging.

through the force feedback. In general, it is difficult to model nano-environment with dynamic perturbations and objects with irregular shapes and sizes, therefore the virtual conditions assumed to acquire the virtual visual information cannot embody the reality conditions.

In addition, uncertainties existing in the AFM system and the nano-environment can cause the positioning biases of AFM tip and there is great potential to enhance the effectiveness and efficiency of nano-manipulation by improving AFM tip positioning precision since a series of positioning points constitute a trajectory of nano-manipulation. Some approaches, from this point of view, have been proposed to achieve precise positioning. The deformation uncertainty of AFM cantilever can cause tip positioning error. An Euller–Bernoulli model based controller of active AFM probe employing Periodic–Output–Feedback law has been designed to control the active AFM cantilever's nominal rigidity and reduce its deformation uncertainty for precise tip positioning of nano-manipulation [9]. Through the capability of dynamically changing the active cantilever's rigidity, the force sensitivity of nano-manipulation system and the accuracy of nano-manipulation can be improved at the same time. However, the controller requires the cantilever to be active and achieves only the displacement curve of probe tip. Recently, a non-vector space control strategy based on compressive feedback has been proposed to improve the accuracy of SPM-based nano-manipulation, in which the set of local images (or compressive data) are used as both the reference input and feedback for a non-vector space closed-loop controllers [10], [11]. This control strategy requires no prior information on features or landmarks of nano-environments and emphasizes on accuracy problem in nano-manipulation, such as nano-measurement and nano-surgery, under several nanometers. The non-vector space control strategy can achieve highly accurate probe motion control while increasing feedback rate utilizing compressive sensing and the Hausdorff distance that treats images as sets and avoids image reconstruction. However, in this control strategy, the initial image and goal image should be sufficiently close to each other with some overlap to guarantee the local stability of the controller. In other words, the goal image should be in the vicinity of the initial image in order to bound the Hausdorff distance. Otherwise, a proper motion planner is needed for trajectory planning. Furthermore, to achieve high accuracy of nano-manipulation, the control strategy requires frequent scanning and the moving step size of the probe is quite small, even less than 1 nm, which is not necessary and time-consuming in many nano-manipulation application. For the destination-oriented and long distances nano-manipulation, such as moving objects from one location to another one, it is difficult to satisfy requirement that the goal image is within the vicinity of the initial image. Additionally, in this case, it is inappropriate to apply the Hausdorff distance to measure the difference between the current location of the objects to be moved and the destination location. Furthermore, instead of accuracy, such nano-manipulation seeks manipulation efficiency and effectiveness with less imaging and larger step size in the process of manipulation. It is imperative to track real-time trajectory of nano-manipulation to adjust tip position and guide manipulation orientation in time.

In this paper, we present a new strategy based on compressive sensing to realize quick real-time tracking of nano-manipulation and build a new kinematic model for objects to be manipulated to overcome the effect of tip positioning and contacting biases on nano-manipulation with AFM based nano-robotic system. The compressive tracking strategy can be used to realize automatic nano-manipulation and improve its accuracy and efficiency.

II. Overview of the Whole Process

The whole process of the proposed tracking strategy consists of four procedures: overall image acquisition, object recognition, nano-manipulation and local image acquisition, as shown in Fig. 1. The procedure of acquiring a goal image is firstly implemented by the traditional scanning model (tapping mode) of AFM. The other procedures comprise an closed iteration loop to solve three key problems: (1) recognition of the target to be manipulated and its desired destination area (where the target object is manipulated or moved to) in the goal image acquired in the first procedure, (2) nano-manipulation of the target object with AFM based nano-manipulation system, guided by the distance vector between the object location and the destination, and (3) acquisition of the local image, based on compressive

sensing, of the new region around the target object in the goal nano-space. The local image is fed back for re-recognition of the target object and its current location. The distance deviation between the new location of the target object and the destination is assessed to guide next nano-manipulation of the object. The iteration loop is repeated until the manipulation task is completed and the target object is moved to the desired destination.

The paper is organized as follows: Section III briefly introduces the method for object recognition using AFM image. Section IV discusses the approach to compressive tracking. The compressive sensing theory, the approach to designing compressive measurement matrix, and the method of local imaging are described in details. Section V presents the automatic process of nano-manipulation. Section VI displays some experiments and results. Section VII concludes the paper.

III. Object Recognition

AFM topographical images encode height information of objects and background of operation nano-space, and the objects can be differentiated from the background using the height information of AFM images. In this study, a target object is recognized by searching sub-areas through the local images and making comparison with the profile of the target object. In details, the target object profile, containing the characteristic height information, is firstly extracted from the goal image, which is acquired by the AFM tapping mode, and the object profile is denoted by a matrix X. Meanwhile, the destination location of the target object to be moved is determined on the goal image, and hence the moving trajectory of object manipulation is planned according to the current and destination locations of the target object. After implementing one nano-manipulation, the target object is moved to a new location, which in general deviates from the planned trajectory due to the nonlinearities and uncertainties during the nano-manipulation. The area where the object is moved to by one nano-manipulation is locally imaged based on compressive sensing. The sub-area, denoted by $\bar{X}$, of the same size as that of the object profile X, is searched through within the local image and then compared with X. The object at the new location is recognized by the following inequality:

$$\left\|X - \bar{X}\right\| \leq \varepsilon, \tag{1}$$

where ε is the threshold for object recognition. Then the new location of the object can be determined and the moving trajectory is re-planned to correct the deviation for the next object manipulation.

IV. Compressive Tracking

In order to observe the environment changes, including the movement of objects, in the nano-space, the topographical image of sample surface needs to be acquired by AFM. However, it is time-consuming to scan the whole sample surface with AFM. In the nano-manipulation with moving the target object from its original location to a destination location, to improve the accuracy and efficiency, it is of great importance to track the object movement and to observe the environment change surrounding the target object only. Therefore it will improve the nano-manipulation effectiveness and efficiency by imaging the local area that contains the target object after one manipulation. Furthermore, it has been demonstrated that AFM imaging rate can be improved with compressive sensing [12], [13]. In this study, local imaging based on compressive sensing is utilized to quickly track the object movement.

Compressive tracking has been widely employed in the field of computer vision to quickly track targets [14], [15]. In these works, the concept of compressive sensing is applied to reduce the dimensionality of feature space after acquisition of video frames and hence improve tracking efficiency. However, for the tracking problem in nano-manipulation, a major part of time is expended in AFM imaging. Therefore, if the time for AFM imaging is significantly reduced, while the features of nano-space are kept, the tracking efficiency will be largely improved. In this study, compressive sensing is utilized in the phase of AFM imaging and AFM imaging rate is significantly improved. The measurement matrix for the compressive imaging is designed so that the features of nano-space are maintained for tracking. The key to the compressive tracking in nano-manipulation, proposed in this study, is the application of compressive sensing during the procedure of local imaging within the closed iteration loop in the nano-manipulation process.

The procedure of the local compressive imaging in the nano-manipulation consists of three main steps: determining the range of local imaging, designing AFM scanning strategy and implementing local imaging based on the compressive sensing. In addition, there exist uncertainties in AFM tip positioning and object localization due to thermal drift in nano-space and nonlinearities of nano-manipulation systems, which cause contacting bias between the AFM tip and the target and result in manipulation deviation. In this study, Gaussian distribution is used to describe the uncertainties of initial AFM positioning and object localization.

Here, some preliminaries of compressive sensing are presented firstly.

A. Compressive Sensing

Compressive sensing has been built upon by Candes *et al.* [16], Donoho [17], and so on, and it is a type of undersampling method that samples blow Nyquist rate to acquire high-resolution image. Central to compressive sensing is a strategy that reconstructs a sparse signal $x \in R^{N\times 1}$ from an observation vector $y \in R^{M\times 1}$ by a linear equation $y = \Phi x$, where $\Phi \in R^{M\times N}$ is a measurement matrix and $M < N$ [16]–[18]. The equation cannot be solved with the classic matrix inversion since it is under-determined and the solution is not unique. However, it has been proven that the minimal l_0-norm problem can be used to reconstruct the sparse signal x with large probability by linear programming under the condition that the signal x is k-sparse (i.e., the signal x contains no more than $k < M$ non-zero entries) and Φ satisfies the restricted isometry property (RIP) condition [19]. Gaussian matrix [20] and Bernoulli matrix [21] are two stable measurement matrices that satisfy the RIP condition. Bernoulli matrix, consisting of 1 and 0, is

chosen as a measurement matrix for local compressive imaging in this study. The minimal l_0-norm problem can be formulated as follows:

$$\hat{x} = \arg\ \min \|x\|_0\ \ \text{s.t.} y = \Phi x. \tag{2}$$

But not all natural signals are sparse, so one of the key steps of compressive sensing is sparse representation of a signal x, by which the signal x can be transformed into a sparse signal s through a special representation matrix Ψ, as shown in the following equation [22],

$$x = \Psi s. \tag{3}$$

It has been proven that the smooth signals can be sparsely represented by Fourier or Wavelet transform, and the signals with bounded total-variation can be sparsely represented by Wavelet transform [23]. In this study, Fourier transform will be used to sparsely represent the original signal because Fourier transform can realize a more sparse representation for the local image and it is easier to implement than Wavelet transform. Denoting $\Phi\Psi$ by Θ, then the linear equation $y = \Phi x$ can be rewritten as follows:

$$y = \Theta s. \tag{4}$$

B. Design of Measurement Matrix

A good measurement matrix is a guarantee to accurately reconstruct sparse signals in compressive sensing, but not all matrices are suitable for signal reconstruction. To better and robustly recover sparse signals, a necessary and sufficient condition is that the measurement matrix Φ satisfies the RIP condition, that is, for any k-sparse signal x,

$$(1-\delta_k)\|x\|^2 \le \|\Phi x\|^2 \le (1+\delta_k)\|x\|^2, \tag{5}$$

where $\delta_k \in (0,1)$ denotes the restricted isometry constant of the matrix Φ [16]. And it has been proven that the Gaussian matrix [20] and the Bernoulli matrix [23] are two stable measurement matrices that satisfy the RIP condition.

However, it is difficult to prove whether the matrix Φ satisfies the RIP condition. The coherence between the measurement matrix Φ and the representation matrix Ψ has been proposed to explore whether the sensing matrix $\Theta = \Phi\Psi$ satisfies the RIP condition [23]. The coherence coefficient between the measurement matrix Φ and the representation matrix Ψ is defined as follows:

$$\mu(\Phi,\Psi) = \sqrt{N} \cdot \max_{1\le j,k\le N} \left|\left\langle \phi_j^T, \psi_k \right\rangle\right|, \tag{6}$$

where ϕ_j and ψ_k denote the row and the column vectors of the matrix Φ and Ψ, respectively. The coherence coefficient $\mu(\Phi,\Psi)$ follows from the linear algebra that $\mu(\Phi,\Psi) \in \left[1, \sqrt{N}\right]$. If Φ and Ψ contain correlated elements, then the coherence coefficient $\mu(\Phi,\Psi)$ is large, and Φ and Ψ are of high coherence; otherwise, the coherence coefficient is small, and Φ and Ψ are of high incoherence. If Φ and Ψ are of high incoherence, then the sensing matrix Θ satisfies the RIP condition with high probability [22], [24] [25].

Nowadays, the compressive sensing theory has been widely utilized in AFM imaging to reduce the time for acquiring topographical images [12], [13], [26]. In these works, the measurement matrix Φ used in AFM imaging is chosen to be a certain form of matrix that has all entries to be either 1 or 0, determining a pixel is sampled with 1 or not with 0 respectively. Furthermore, in order to save imaging time, each row of the matrix contains just one entry to be 1 and other entries to be 0, and all rows are different from each other. Therefore it is obvious that the row vectors of the measurement matrix Φ are orthonormal.

For a measurement matrix Φ in AFM imaging defined as above, a Fourier transformation

$$\Psi = \frac{1}{\sqrt{N}} \begin{bmatrix} \omega^0 & \omega^0 & \omega^0 & \cdots & \omega^0 \\ \omega^0 & \omega^1 & \omega^2 & \cdots & \omega^{N-1} \\ \vdots & \vdots & \vdots & \ddots & \vdots \\ \omega^0 & \omega^{N-1} & \omega^{2N-1} & \cdots & \omega^{(N-1)^2} \end{bmatrix},$$

where $\omega = \exp\left(-i\frac{2\pi}{N}\right)$, is chosen as the representation matrix, then the coherence coefficient $\mu(\Phi,\Psi) = 1$. Hence Φ and Ψ have the least coherence and are of high incoherence. Hence the sensing matrix $\Theta = \Phi\Psi$ satisfies the RIP condition with high probability [24].

C. Determination of the Range of Local Imaging

Because of the effects of thermal drift and nonlinearities of AFM robotic system, there exist uncertainties in AFM tip positioning and object localization, which cause contacting biases when AFM tip approaches the object for manipulation and result in moving deviations from the planned trajectory along which the object is manipulated. Hence, the range of local imaging should be enough to cover the whole target object to be manipulated with the contacting biases and moving deviations due to the perturbation of thermal drift and system nonlinearities. So the range of local imaging is decided by not only the size of the target object but also the effect of uncertainties. It has been demonstrated that the uncertainties obey Gaussian distribution [5]. Assume that the total uncertainty for both AFM tip positioning and object localization is Gaussian denoted by $x \sim N(0,\sigma)$, then $[x_c - x_0, x_c + x_0]$ represents the range within which AFM tip contacts the object with probability of $\mathrm{P}\{|x - x_c| < x_0\} > 99\%$, where x_c is the desired point where AFM tip approaches to and $x_0 = 3\sigma$. So the step size of one nano-manipulation and the range of local imaging can be calculated as below, and Fig. 2 shows the sketch for the calculation.

As shown in Fig. 2(a), assume that the local image to be acquired is square, let *a* denote its side length, *L* the step size of each nano-manipulation, and *V* the moving speed of AFM tip in the nano-manipulation, then we have,

$$a = 2(r + x_0 + \varepsilon), \tag{7}$$

where r is the radius of the object and ε is the tolerance constant, which is to ensure that the local image to be acquired can contain all features of the target object. Then, we analyze the kinematic

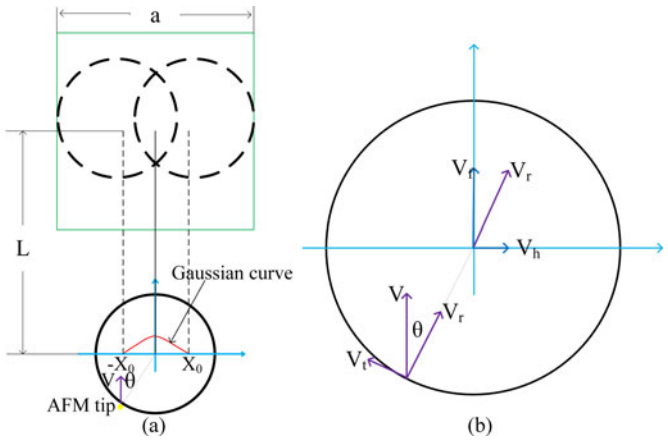

Fig. 2. The calculation of the manipulation distance and the local imaging range. (a) The locations of the object by one step of manipulation. The solid circle denotes the current location of the object, and the dashed circles denote the possible location of the object after one step of manipulation. Green box is the boundary of local image to be acquired; (b) The kinematic model of the target object during manipulation.

model of nano-manipulation, as shown in Fig. 2(a), and we conclude that, for any time period Δt and the angle θ_t at the time t,

$$\begin{cases} \Delta L = V\ \cos^2\ \theta_t\ \Delta t \\ \Delta H = V\ \ \sin\theta_t\ \cos\theta_t\ \Delta t, \end{cases} \tag{8}$$

where ΔL and ΔH is moving distances of the object for the time period Δt along the moving direction of AFM tip and the lateral direction, which is perpendicular to the moving direction, respectively. So, at any time t_0,

$$\begin{cases} L = \int_0^{t_0} V\cos^2\theta_t\, dt \\ H = \int_0^{t_0} V\sin\theta_t\,\cos\theta_t\, dt \\ \theta_t \le \arcsin\dfrac{H+x_0}{r} \\ H \le \min\left\{2x_0 + 2\varepsilon, r - x_0\right\}. \end{cases} \tag{9}$$

Simplifying the equation (9), then we have the following inequality:

$$\begin{cases} L = \dfrac{H}{\ln r - \frac{1}{2}\ln\left(r^2 - (H+x_0)^2\right)} \\ H \le \min\left\{2x_0 + 2\varepsilon, r - x_0\right\}, \end{cases} \tag{10}$$

which gives the constraint on how far the object can be moved by one step of nano-manipulation.

Another key problem for local imaging is to determine the center of the local image to be acquired after one nano-manipulation. The center of the local image is determined by the center of the last local image that has been acquired and the last manipulation. As shown in Fig. 3, the center of the local image is calculated by the following equation:

$$\mathrm{O}_i = \mathrm{O}_{i-1} + \boldsymbol{L}_{i-1}, \tag{11}$$

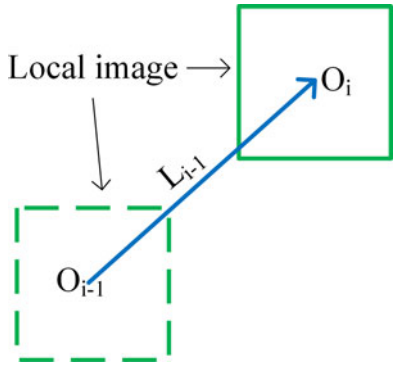

Fig. 3. Method to determine the center of the local imaging after one step of manipulation. The dashed block and solid block denote the range of last local imaging and the current local imaging, respectively, and the bold line with the arrow denotes the moving vector for the last step of manipulation.

where O_i denotes the current center of the local image to be acquired, O_{i-1} is the center of the last local image acquired, $\boldsymbol{L}_{i-1}$ is the moving vector of the object under the last nano-manipulation, where $\|\boldsymbol{L}_{i-1}\| = L$ is subject to the constraint defined by inequality (10).

Once the center O_i is determined, the range of the local imaging is achieved by a square centered at O_i with sides of length a.

D. Local Imaging

The imaging time to acquire surface topographical image with AFM is significantly dependent on the image size and resolution. For an image of constant size and resolution, the shorter distance AFM tip moves, the faster AFM acquires the image. It is worth focusing attention on both reduction of AFM sampling points and optimization of scanning path for shorter movement distance of AFM tip to save the imaging time. Compressive sensing is such an approach to achieving high resolution image with lower sampling rate, and, in this study, the measurement matrix Φ for compressive sensing is chosen as discussed above, that is, only one element in each row of the measurement matrix is 1 and others are 0.

Given the measurement matrix Φ, a scanning strategy can be made to further save imaging time by optimizing the scanning path for shorter distance. In details, a scanning matrix is formed from the measurement matrix Φ by reshaping each row vector of Φ into a matrix with the same dimensions as that of local image to be scanned and then superimposing these matrices onto one matrix for scanning with AFM. The scanning matrix contains M entries to be 1 and rest entries to be 0, and only those points corresponding to 1 on the sample surface will be scanned.

A scanning strategy is generated by planning scanning path for AFM probe tip with a certain rule. Several measurement matrices have been proposed to generate the scanning strategy, all of which are proved to be capable of recovering high resolution images with less time through AFM imaging experiments [13], [26]. Three typical scanning strategies are shown in Fig. 4. The square scanning strategy (see Fig. 4(a)) and the spiral scanning strategy (see Fig. 4(b)) take regular scanning paths, and they

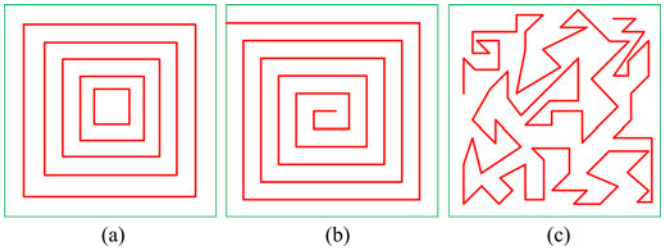

Fig. 4. The scanning strategies in AFM imaging. The red lines denote the AFM tip scanning trajectory on the sample surface and the green square is the boundary of the local image to be scanned. (a) The square scanning strategy; (b) The spiral scanning strategy; (c) The optimal scanning strategy.

are easier to implement for both hardware and software systems in practice. But the tip scanning paths are not the shortest. Furthermore, these two strategies may cause information loss when the samples are small. Fig. 4(c) is generated based on the measurement matrix, as stated above, and its scanning path is optimized for shortest tip moving distance by solving travelling salesman problem. With this strategy, images can be acquired with shorter time while the image information can be kept by taking advantage of compressive sensing. The optimal scanning strategy is chosen for local compressive sensing.

V. Nano-Manipulation

The critical problem of nano-manipulation is to determine the moving orientation and distance for one step of nano-manipulation. The moving orientation of manipulation is determined by the relative position of the current location of the object and the destination location, and the moving distance is subject to both the inequality (10) and the actual distance from the current location to the destination. As shown in Fig. 5, O_1, O^* and O_i denote the object center at the original location, the destination location, and the current location before the ith nano-manipulation, respectively; $\boldsymbol{D}_i$ is the distance vector from the current location O_i to the destination location O^*, and $\boldsymbol{L}_i$ is the moving vector from the current location to the next location by the ith nano-manipulation. It is required that the moving vector $\boldsymbol{L}_i$ points to the destination, namely $\boldsymbol{L_i}/\left\|\boldsymbol{L}_i\right\| = \boldsymbol{D_i}/\left\|\boldsymbol{D}_i\right\|$. The moving distance $\left\|\boldsymbol{L}_i\right\|$ is subject to the constraint defined by inequality (10). Then the nano-manipulation strategy is designed by the following procedures:

Step 1. Acquiring the object center of current location O_i for the ith nano-manipulation;
Step 2. Calculating the distance vector $\boldsymbol{D}_i$, where $\boldsymbol{D}_i = \boldsymbol{O}^* - \boldsymbol{O}_i$, by which the moving orientation is determined for moving vector $\boldsymbol{L}_i$;
Step 3. Determining the moving distance for moving vector $\boldsymbol{L}_i$ through comparing the actual distance, $\left\|\boldsymbol{D}_i\right\|$, from the current location to the destination location and the step size limitation L defined in inequality (10): if $\left\|\boldsymbol{D}_i\right\| > L$, then $\boldsymbol{L}_i = \boldsymbol{D_i}/\left\|\boldsymbol{D}_i\right\| * L$; otherwise, $\boldsymbol{L}_i = \boldsymbol{D}_i$.

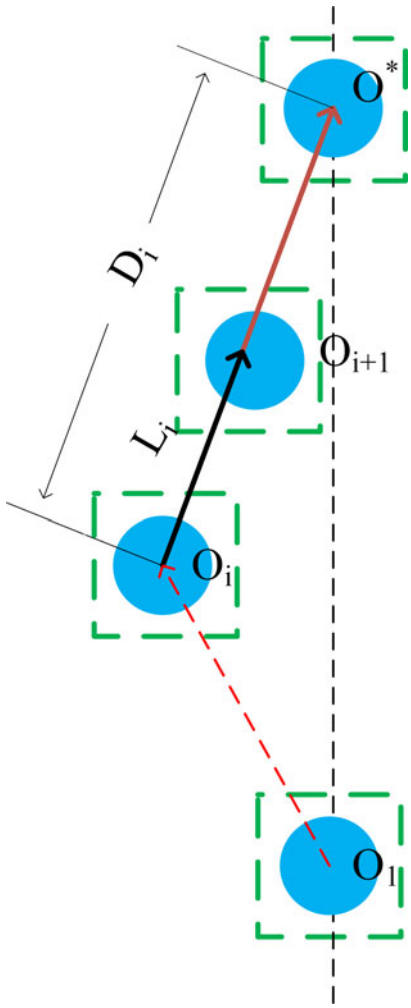

Fig. 5. The sketch of nano-manipulation. The solid circle denotes the object and the dotted box is the range of local image.

VI. Implementation and Experimental Results

A. Overview

Two experiments of object manipulation at nano-scale were carried out to illustrate the validity of nano-manipulation strategy with real-time tracking based on compressive sensing. All the tests were implemented with Dimension 3100 AFM (Veeco Inc.), and the software of nano-manipulation and local imaging were designed by our lab. The objects to be manipulated in the experiments include the nanoparticles with regular shape and viruses with irregular shape. The procedures of both nano-manipulation and compressive tracking are similar, which are briefly described as follows:

Step 1. Acquiring a goal image containing the interest region;
Step 2. Recognizing the object to be manipulated and the destination location in the goal image as described in Section III. And the features of the target object and the destination location are stored into two matrices respectively;
Step 3. Calculating the relative distance vector $\boldsymbol{D}_i$ between the current location and the destination location of the object, then setting the moving vector $\boldsymbol{L}_i$including both moving distance

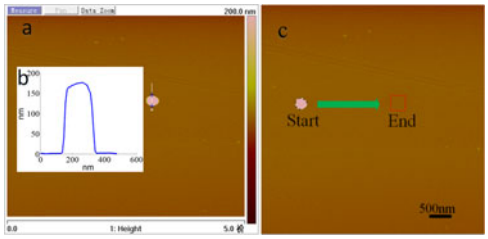

Fig. 6. The goal image and object recognition. (a) The goal image with the size of 5 × 5 μm; (b) The profile of the nanoparticle of interest with a diameter of 200 nm; (c) The image with an object recognized. The black dotted circles denote the object at the starting location, while the red solid square box is the destination location.

and moving orientation, for one step of manipulation based on Section V;

Step 4. Moving AFM tip to the object boundary and pushing the object by the moving vector $\boldsymbol{L}_i$ obtained in step 3, with the moving speed of V;

Step 5. Determining the center and range of the local image to be acquired based on the equation (7) and (11), then acquiring the local image based on the compressive sensing strategy. Finally, the new location of the object is determined and marked onto the goal image;

Step 6. Going back to step 2 and repeating step 2 to step 5 until the object is moved to the destination location, then the whole nano-manipulation with nano-tracking is finished.

B. The Experiment of Nanoparticle Manipulation

In the first experiment, the polystyrene nanoparticles of diameter 200 nm diluted in deionized water were used for sample preparation. A droplet of diluted sample solution was placed onto the surface of a gold electrode, which was plasma surface treated for about 5 min in the oxygen environment with the volume flow rate of 20 sccm, and dried in the room temperature for about 30 min. The tapping mode was used in AFM scanning and the goal image with interest region was acquired, as shown in Fig. 6(a) and (b). The starting location and the destination where the object to be moved are shown in Fig. 6(c).

In this experiment, two nano-manipulations were implemented by moving nano-objects to the destination at different directions, one is with the destination on the horizontal direction, and the other is with the destination on the non-horizontal direction. It is reasonable that the nano-manipulation to a destination on the vertical direction is similar to that on the horizontal direction. Considering the uncertainties of initial position of AFM tip and the requirements of stable nano-manipulation and accurate tracking, some parameters were set first. We set the parameter of Gaussian distribution $\sigma = 10\,\mathrm{nm}$ based on [5], [27], the step size limitation of manipulation $L = 600\,\mathrm{nm}$ for horizontal manipulation and $L = 300\,\mathrm{nm}$ for non-horizontal manipulation in inequality (10), the manipulation speed $V = 300\,\mathrm{nm}/s$, and the tolerance constant $\varepsilon = 20\,\mathrm{nm}$. So the side length of the square range for local image is set to be $a = 300\ \mathrm{nm}$ based on equation (7). In order to achieve the real-time tracking function, it is better to spend less time on local imaging. So, compressive sensing was employed in local imaging to acquire the object features with far less sampling. In this experiment, the size of local image is $300 \times 300\,\mathrm{nm}$ and the image resolution is 32×32. With traditional AFM imaging, the image of the object was acquired through scanning all the sample points, row by row, within the range of local imaging. With compressive imaging method, only 30% sample points are scanned with the minimized scanning path to acquire the local image while keeping the characteristic features of the object of interest. The local images of an object of interest acquired by these two methods are shown in Fig. 7(a) and (b), respectively, and it is obvious that the object profile can be identified by the contours extracted from both images, as shown in Fig. 7(c) and (d). The optimal scanning strategy based on the chosen measurement matrix is shown in Fig. 7(e). Apparently the time for local imaging with the compressive imaging approach is up to two thirds less than the time with the traditional imaging method, as shown in Fig. 7(f).

The tracking results at all steps were recorded onto the goal image marked with solid circle and strung with solid line, for two nano-manipulations along different moving directions, as shown in Fig. 8(a) for the horizontal direction and Fig. 8(c) for the non-horizontal direction. The distances between the objects and the destination locations were calculated at each step, as shown in Fig. 8(b) and (d) for the two nano-manipulations. The compressive tracking during the process of nano-manipulation is completed. The two manipulations along these two directions were compared and it is obvious that the nano-manipulation along the horizontal direction (see Fig. 8(a)) is much easier than that along the non-horizontal direction (see Fig. 8(c)) since the deviations along the horizontal direction during the nano-manipulation are much smaller than the deviations along the non-horizontal direction. However, even in the manipulation along non-horizontal direction, the deviation at each step can be corrected by the real-time compressive tracking and the object can be accurately moved to the destination. Therefore it is validated that the compressive tracking can promote the nano-manipulation of an object to any destination in the nano-space with much less time.

C. The Experiment of Virus Manipulation

In the first experiment, the nano-object to be manipulated is hard and has regular shape. During the nano-manipulation, the size and shape of the object keep unchanged. However, in practice, many nano-objects, such as biological sample, to be manipulated are soft and irregular in shape, and their size could vary during the manipulation. Therefore, another experiment is needed to validate the compressive tracking for nano-manipulation of soft and irregular samples.

The second experiment was carried out to manipulate a virus with compressive tracking. The virus is one type of adenovirus Ad5-EGFP (VGTC Inc., China), which lacks capability of self-replication and infectivity by removing the E1 and E2 region of DNA.

The virus with concentration $5.12 \times 10^{10}/\mathrm{mL}$ diluted in deionized water was used for sample preparation. A droplet of diluted sample solution was placed onto the surface of a gold electrode, which was plasma surface treated about 5 min in the oxygen environment with the volume flow rate of 20 sccm, and dried in room temperature for about 1 h. Then, the surface of

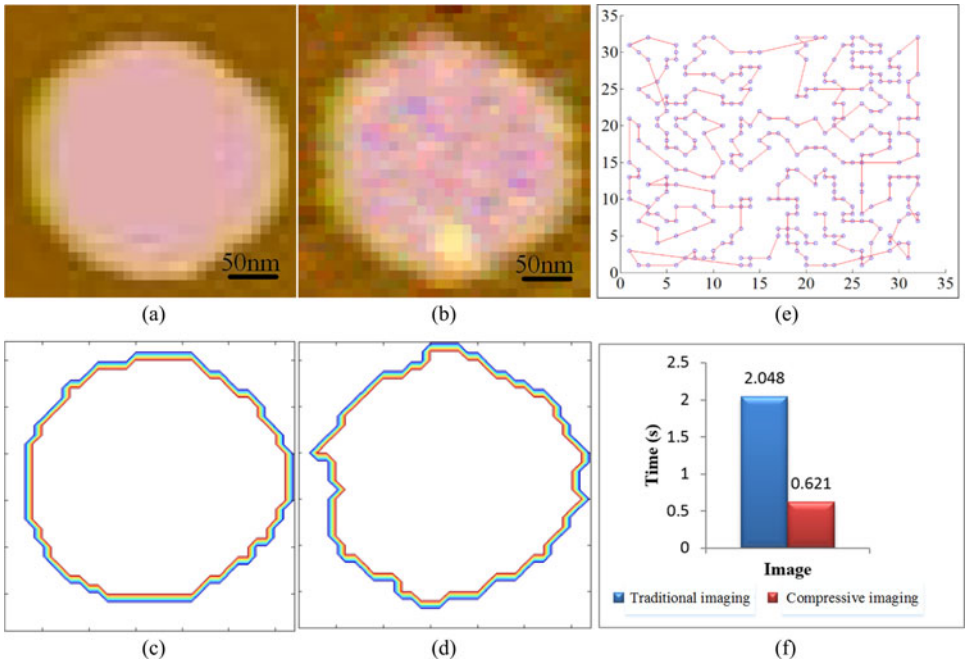

Fig. 7. The local imaging and object recognition. (a) The local image acquired with traditional imaging, i.e., sampling all points with row by row at resolution of 32×32; (b) The local image acquired with compressive imaging, i.e., sampling 307 stochastic points within the range of local imaging; (c) and (d) The contours of the object extracted from the local images (a) and (b), respectively; (e) The optimal scanning strategy for AFM tip movement with the shortest path based on the chosen measurement matrix, the blue dots represent the points to be sampled in the sample surface, determined by the entries of 1 in the scanning matrix, and the red curve represents the scanning trajectory of AFM tip; (f) The comparison of scanning times with traditional imaging and compressive imaging.

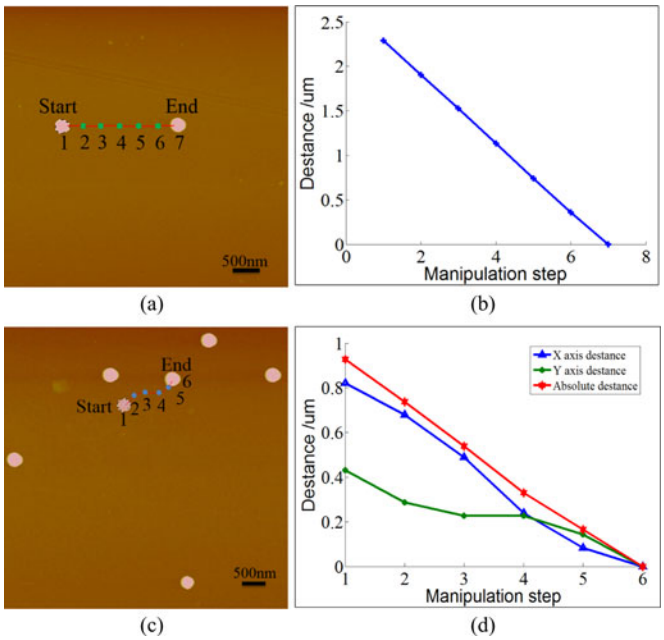

Fig. 8. The tracking process of the nanoparticle manipulation with compressive tracking. (a) and (c) The tracking of two nano-manipulations along the horizontal direction and the non-horizontal direction respectively; (b) and (d) The distance between the object and destination location at each step of manipulation corresponding the manipulation processes (a) and (c), respectively. Especially, for the manipulation process along the non-horizontal direction, the distances in *X*-axis and *Y*-axis are given too.

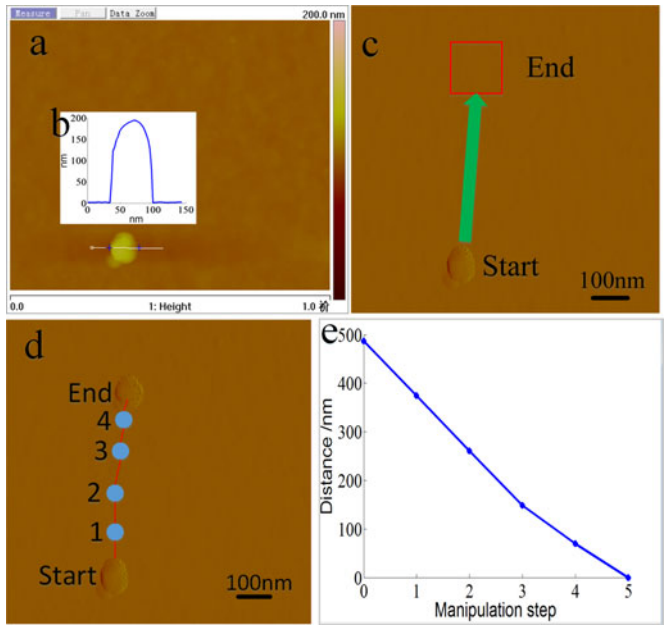

Fig. 9. The tracking process of nano-manipulation of a virus (a) The goal image with the size 1×1 μm; (b) The profile of one virus of interest in the image (a), and the diameter of the virus is less than 100 nm; (c) The image with one virus recognized. The red solid box is the destination location; (d) The tracking process of manipulation of the virus; (e) The distance between the virus and the destination location at each step of manipulation.

sample was washed gently with a spot of deionized water, and dried again in room temperature for about 30 min. The tapping mode was used in AFM scanning and the goal image with interest region was acquired, as shown in Fig. 9(a) and (b). The diameter of the virus is less than 100 nm, so the size of the virus is set to be 100 nm. The starting location and the destination where the virus to be moved are shown in Fig. 9(c).

Unlike rigid nanoparticle, there is a deformation between the tip and the virus during the contact process, so the tip and virus

move gradually to the target location with less deviation, so the Gaussian distribution is smaller than that for hard nanoparticle, and the parameter $\sigma = 5\,\mathrm{nm}$ was chosen according to the repeated experiments. The other parameters were set as: the step size of manipulation $L = 150\,\mathrm{nm}$, the manipulation speed $V = 300\,\mathrm{nm/s}$, and the tolerance constant $\varepsilon = 5\,\mathrm{nm}$. So, the side length of the square range for local image is set to be $a = 120\,\mathrm{nm}$ based on equation (7). Similar to the experiment for manipulating the nano-particle described as above, the virus was pushed with real-time compressive tracking from the original location to the destination location, as shown in Fig. 9(d) and (e). Similar to the first experiment for manipulation with hard and regular nano-objects, the deviation at every step of manipulation can be corrected with the compressive tracking and the virus was successfully moved to the designed destination. Therefor it is validated that the compressive tracking enhances the effectiveness and efficiency of manipulation for soft and irregular nano-objects as well as those hard and regular objects.

VII. Conclusion

AFM-based manipulation system is a promising system for manipulating objects at nano-scale and fabricating nanostructures. The kinematic model assures that the tip can always contact the object being manipulated and deviation of the object from the pre-designed path by one step manipulation is controlled within a reasonable range. The model also provides the range for local compressive imaging for next step of manipulation. The procedure of local imaging is crucial in the proposed tracking strategy since the major time is reduced by compressive sensing, and with this strategy, the tracking time is significantly reduced and the deviation of the object from the pre-designed path can be corrected in time. Two experiments with both hard, round nano-particles and soft, irregular virus were implemented to validate the real-time compressive tracking strategy. The success of the experiments proves that this compressive tracking approach requires no priori knowledge about the system, environment and objects being manipulated and that the approach works for both hard, regular objects and soft, irregular samples. Therefore the compressive tracking strategy can be widely applied in nano-manipulation. In addition, the compressive tracking strategy can help realize automation of nano-manipulation and improve its accuracy and efficiency.

References

[1] G. Binnig, C. F. Quate, and C. Gerber, "Atomic force microscope," *Phys. Rev. Lett.*, vol. 56, pp. 930–933, 1986.

[2] A. A. G. Requicha, C. Baur, A. Bugacov, B. C. Gazen, B. Koel, A. Madhukar, T. R. Ramachandran, R. Resch, and P. Will, "Nanorobotic assembly of two-dimensional structures," in *Proc. IEEE Int. Conf. Robot. Autom.*, 1998, vols. 1–4, pp. 3368–3374.

[3] T. Junno, K. Deppert, L. Montelius, and L. Samuelson, "Controlled manipulation of nanoparticles with an atomic-force microscope," *Appl. Phys. Lett.*, vol. 66, pp. 3627–3629, Jun. 26, 1995.

[4] S. Darwich, K. Mougin, A. Rao, E. Gnecco, S. Jayaraman, and H. Haidara, "Manipulation of gold colloidal nanoparticles with atomic force microscopy in dynamic mode: Influence of particle-substrate chemistry and morphology, and of operating conditions," *Beilstein J. Nanotechnol.*, vol. 2, pp. 85–98, Feb. 4, 2011.

[5] J. Hou, L. Q. Liu, Z. Y. Wang, Z. D. Wang, N. Xi, Y. C. Wang, C. D. Wu, Z. L. Dong, and S. Yuan, "AFM-based robotic nano-hand for stable manipulation at nanoscale," *IEEE Trans. Autom. Sci. Eng.*, vol. 10, no. 2, pp. 285–295, Apr. 2013.

[6] M. Sitti and H. Hashimoto, "Tele-nanorobotics using an atomic force microscope as a nanorobot and sensor," *Adv. Robot.*, vol. 13, pp. 417–436, 1999.

[7] X. Tian, Y. Wang, N. Xi, Q. Liu, N. Jiao, and Z. Dong, "AFM based MWCNT nanomanipulation with force and visual feedback," *J. Nanosci. Nanotechnol.*, vol. 9, pp. 1647–1650, 2004.

[8] N. Jiao, L. Liu, X. Tian, Y. Wang, N. Xi, and Z. Dong, "An interactive nanomanipulation system with force and visual feedback," *Robot*, vol. 28, pp. 279–284, 2006.

[9] L. Hao, J. Zhang, and N. Xi, "Design and implementation of precise position controller of active probe of atomic force microscopy for nanomanipulation," *Chin. Sci. Bull.*, vol. 53, pp. 2090–2096, 2008.

[10] B. Song, J. G. Zhao, N. Xi, H. Z. Chen, K. W. C. Lai, R. G. Yang, and L. L. Chen, "Compressive feedback-based motion control for nanomanipulation-theory and applications," *IEEE Trans. Robot.*, vol. 30, no. 1, pp. 103–114, Feb. 2014.

[11] B. Song, J. G. Zhao, N. Xi, K. W. C. Lai, R. G. Yang, H. Z. Chen, and C. G. Qu, "Non-vector space control for nanomanipulations based on compressive feedbacks," in *Proc. IEEE Int. Conf. Robot. Autom.*, 2012, pp. 2767–2772.

[12] G. Li, P. Li, Y. Wang, W. Wang, N. Xi, and L. Liu, "Efficient imaging and real-time display of scanning ion conductance microscopy based on block compressive sensing," *Int. J. Optomechatron.*, vol. 8, pp. 218–227, 2014.

[13] B. Song, N. Xi, R. G. Yang, K. W. C. Lai, and C. G. Qu, " Video rate atomic force microscopy (AFM) imaging using compressive sensing," in *Proc. IEEE 11th Int. Conf. Nanotechnol.*, 2011, pp. 1056–1059.

[14] K. Zhang, L. Zhang, and M.-H. Yang, "Real-time compressive tracking," in *Proc 12th Eur. Conf. Comput. Vis.*, 2012, pp. 864–877.

[15] Z. Mao, J. J. Yuan, Z. R. Wu, J. S. Qu, and H. Y. Li, "Real-time compressive tracking based on online feature selection," in *Proc. Int. Conf. Comput. Sci. Inf. Technol.*, 2014, vol. 255, pp. 431–438.

[16] E. J. Candes, J. Romberg, and T. Tao, "Robust uncertainty principles: Exact signal reconstruction from highly incomplete frequency information," *IEEE Trans. Inf. Theory*, vol. 52, no. 2, pp. 489–509, Feb. 2006.

[17] D. L. Donoho, "Compressed sensing," *IEEE Trans. Inf. Theory*, vol. 52, no. 4, pp. 1289–1306, Apr. 2006.

[18] Y. Tsaig and D. L. Donoho, "Extensions of compressed sensing," *Signal Process.*, vol. 86, pp. 549–571, Mar. 2006.

[19] E. J. Candes, "The restricted isometry property and its implications for compressed sensing," *Comptes Rendus Math.*, vol. 346, pp. 589–592, 2008.

[20] E. J. Candes and T. Tao, "Decoding by linear programming," *IEEE Trans. Inf. Theory*, vol. 51, no. 12, pp. 4203–4215, Dec. 2005.

[21] E. C. T. Tao, "Near optimal signal recovery from random projections universal encoding strategies," *IEEE Trans. Inf. Theory*, vol. 52, no. 12, pp. 5406–5425, Dec. 2006.

[22] R. G. Baraniuk, "Compressive sensing," *IEEE Signal Process. Mag.*, vol. 24, no. 4, pp. 118–124, Jul. 2007.

[23] E. J. Candes and T. Tao, "Near-optimal signal recovery from random projections: Universal encoding strategies?" *IEEE Trans. Inf. Theory*, vol. 52, no. 12, pp. 5406–5425, Dec. 2006.

[24] E. J. Candes and M. B. Wakin, "An introduction to compressive sampling," *IEEE Signal Process. Mag.*, vol. 25, no. 2, pp. 21–30, Mar. 2008.

[25] E. Candes and J. Romberg, "Sparsity and incoherence in compressive sampling," *Inverse Probl.*, vol. 23, pp. 969–985, Jun. 2007.

[26] S. B. Andersson and L. Y. Pao, "Non-raster sampling in atomic force microscopy: A compressed sensing approach," in *Proc. Amer. Control Conf.*, 2012, pp. 2485–2490.

[27] Z. Y. Wang, L. Q. Liu, Y. C. Wang, Z. D. Wang, N. Xi, J. Hou, W. X. Wang, and S. Yuan, "Stable nanomanipulation using atomic force microscopy: A virtual nanohand for a robotic nanomanipulation system," *IEEE Nanotechnol. Mag.*, vol. 7, no. 4, pp. 6–11, Dec. 2013.

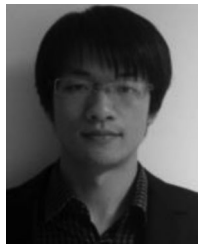

Gongxin Li received the B.S. degree in mechatronics engineering from Shantou University, Shantou, China, in 2011. He is currently working toward the Ph.D. degree at the State Key Laboratory of Robotics, Shenyang Institute of Automation, Chinese Academy of Sciences, Shenyang, China.

His current research interests include compressive sensing, image processing, biological vision, and nanomanipulation based on nanorobots.

Wenxue Wang (M'06) received the B.Sc. degree in automatical control from the Beijing Institute of Technology, Beijing, China, in 1996, the M.Sc. degree in control theory from the Institute of Systems Science, Chinese Academy of Sciences, Beijing, in 1999, and the D.Sc. degree in systems science and mathematics from Washington University in St. Louis, St. Louis, MO, USA, in 2006.

He is currently a Professor at the Shenyang Institute of Automation, Chinese Academy of Sciences, Shenyang, China. His research interests include nanorobotics, intelligent control, and compressive sensing, computational and systems biology.

Yuechao Wang (M'12) received the M.S. degree in pattern recognition and intelligent control from the Shenyang Institute of Automation, Chinese Academy of Sciences, Shenyang, China, in 1987, and the Ph.D. degree in mechatronic engineering from the Harbin Institute of Technology, Harbin, China, in 1999.

Since 1987, he has been with the Shenyang Institute of Automation, Chinese Academy of Sciences, where he is currently a Professor. His current research interests include robot control, multirobot systems, and micronano manipulation.

Shuai Yuan received the B.S. and M.S. degrees from Shenyang Jianzhu University, Shenyang, China, in 2000 and 2003, respectively, and the Ph.D. degree in pattern recognition and intelligent system from the Graduate School of the Chinese Academy of Sciences, Beijing, China, in 2012.

He is currently a Postdoctoral Researcher with the Shenyang Institute of Automation, Chinese Academy of Sciences, Shenyang. He is also an Associate Professor with the Shenyang Jianzhu University. His research interests include nanorobotics, intelligent control, and image processing.

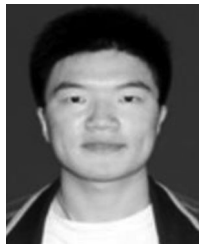

Wenguang Yang received the B.S. degree in measurement and control technology and instrumentation from Yantai University, Shandong, China, in 2011. He is currently working toward the Ph.D. degree at the State Key Laboratory of Robotics, Shenyang Institute of Automation, Chinese Academy of Sciences, Shenyang, China. His current research interests include bioprinting, microfabrication, tissue engineering, and nanomanipulation based on nanorobots.

Ning Xi (F'07) received the D.Sc. degree in systems science and mathematics from Washington University in St. Louis, St. Louis, MO, USA, in 1993, and the B.S. degree in electrical engineering from the Beijing University of Aeronautics and Astronautics, Beijing, China.

He is the University Distinguished Professor and John D. Ryder Professor of electrical and computer engineering with Michigan State University, East Lansing, MI, USA. He currently serves as the Head and the Chair Professor at the Department of Mechanical and Biomedical Engineering, City University of Hong Kong, Hong Kong. His research interests include robotics, manufacturing automation, micro/nano manufacturing, nanosensors and devices, and intelligent control and systems.

Lianqing Liu (M'09) received the B.S. degree in industry automation from Zhengzhou University, Zhengzhou, China, in 2002, and the Ph.D. degree from the Shenyang Institute of Automation, Chinese Academy of Sciences, Shenyang, China, in 2009.

He is currently a Professor at the Shenyang Institute of Automation, Chinese Academy of Sciences. His current research interests include nanorobotics, intelligent control, and biosensors.

Dr. Liu received the Early Government/Industrial Career Award by the IEEE Robotics and Automation Society in May 2011, the Lu Jiaxi Young Scientist Award of the Chinese Academy of Sciences in January 2011, and the President Award of the Chinese Academy of Sciences in 2009.